Available online at www.sciencedirect.com
ScienceDirect
International Journal of Thermal Sciences 47 (2008) 695–708
International Journal of Thermal Sciences
www.elsevier.com/locate/ijts

# Thermal diffusivity measurements of metastable austenite during continuous cooling

P. Matteis *, E. Campagnoli [b], D. Firrao [a], G. Ruscica [b]

[a] *Dip. di Scienza dei Materiali ed Ingegneria Chimica, Politecnico di Torino, Italy*
[b] *Dip. di Energetica, Politecnico di Torino, Italy*

Received 14 July 2006; received in revised form 26 June 2007

Available online 7 August 2007

**Abstract**

The thermal diffusivity of the metastable undercooled austenite is relevant for the quantitative analysis of the carbon and low-alloy steel quench. The standard laser-flash method requires prior thermal equilibrium between the sample and the furnace, which may not be possible to achieve without allowing the metastable phase to transform. Nevertheless, depending upon the steel's hardenability, the thermal transient due to a laser pulse may be much shorter than a cooling transient sufficiently steep to prevent the transformation of the austenite. In one such case, flash measurements were performed during continuous sample cooling and the thermal diffusivity of the metastable austenite was determined by using an extension of the standard analytical model. The adopted analytical model and data reduction procedure are described and the limitations and uncertainties of this method are discussed, also with the aid of a non-linear numerical simulation. The measured thermal diffusivity of the undercooled low-alloy austenite decreases linearly from $5.4 \cdot 10^{-6}$ m$^2$ s$^{-1}$ at 1133 K to $4.3 \cdot 10^{-6}$ m$^2$ s$^{-1}$ at 755 K; this trend is in broad agreement with one previous set of measurements upon a low-alloy undercooled austenite and with a large number of previous standard measurements upon stable (high-alloy) austenitic stainless steels.


*Keywords:* Metastable phase; Low-alloy austenite; Thermal diffusivity; Flash method; Analytical model; Continuous cooling; Steel quenching; Theoretical; Experimental

## Introduction

The pointwise microstructure and the subsequent in-service mechanical properties of a steel component depend primarily upon its heat treatment. Among the steel heat treatments, the quench, being a transient process, is most sensitive to the cooling rate, and consequently to the surface heat transfer phenomena, to the component size and shape, and to the steel's thermal diffusivity[1] and specific heat capacity [1].

The early quantitative methods to estimate quench results [2,3], that are still employed in the industry for a first estimate, were based upon analytical solutions of the heat flux inside geometrically simple bodies. The steel's thermophysical properties and the surface heat-transfer coefficient were considered constant and the pointwise as-quenched hardness was assumed to depend solely upon a parameter (a cooling rate or an half-cooling time) obtained from each cooling curve. In these methods only a rough (effective) approximation of the steel's thermophysical properties could be introduced, because their dependence upon the temperature and upon the phase transformations had to be neglected; therefore, accurate and specific measurements were needless.

On the contrary, present thermo-metallurgical, non-linear, transient, finite-elements models allow to perform coupled simulations of the heat conduction and of the metallurgical phase transformations [4,5]; therefore precise temperature- and

* Corresponding author. Address: Dip. di Scienza dei Materiali ed Ingegneria Chimica, Politecnico di Torino, Corso Duca degli Abruzzi, 24, 10129 Torino, Italy. Tel.: +390115644711; fax: +390115644699.
*E-mail address:* paolo.matteis@polito.it (P. Matteis).

[1] Defined as $\alpha = k/(\rho \cdot c_p)$, being $k$ the thermal conductivity, $\rho$ the density and $c_p$ the specific heat capacity.

1290-0729/$ – see front matter 
doi:10.1016/j.ijthermalsci.2007.06.014

**Nomenclature**

| | | |
|---|---|---|
| $A$ | constant temperature term defined in Eq. (10) | K |
| $B$ | cooling rate defined in Eq. (5) | $K\,s^{-1}$ |
| $C$ | heat capacity | $J\,K^{-1}$ |
| $c_p$ | specific heat capacity | $J\,K^{-1}\,kg^{-1}$ |
| $D$ | heat loss variation parameter defined in Eq. (20) | |
| $E$ | surface heat flux (emissive power) | $W\,m^{-2}$ |
| Erf | error function | |
| $f(\ldots)$ | dimensionless analytic function | |
| $k$ | thermal conductivity | $W\,m^{-1}\,K^{-1}$ |
| $L$ | sample thickness | m |
| $\mathcal{L}_u$ | unilateral Laplace transform operator | |
| $q$ | absorbed pulse energy per surface unit | $J\,m^{-2}$ |
| $Q_a$ | absorbed pulse energy | J |
| $Q_i$ | incident pulse energy | J |
| $R$ | interpolation root mean square residual | K |
| $S$ | section area | $m^2$ |
| $s$ | complex Laplace variable | $s^{-1}$ |
| $S_N$ | partial sum (until the $N$th term of a series) | |
| $T$ | temperature | K |
| $\overline{T}$ | spatial average temperature | K |
| $\overline{\overline{T}}$ | spatial and temporal average temperature | K |
| $t$ | time | s |
| $T_0$ | initial temperature | K |
| $t_0$ | pulse time | s |
| $t_c$ | characteristic time defined in Eq. (5) | s |
| $T_f$ | furnace temperature | K |
| $t_p$ | laser pulse duration | s |
| $u(\ldots)$ | unitary step function | |
| $x$ | position inside the sample | m |
| $Z$ | cooling-related spatial temperature difference $z(L/2) - z(0)$ | K |
| $z$ | cooling-related spatial temperature term defined in Eq. (5) | K |

*Greek symbols*

| | | |
|---|---|---|
| $\alpha$ | thermal diffusivity | $m^2\,s^{-1}$ |
| $\delta$ | thin layer thickness | m |
| $\delta(\ldots)$ | Dirac $\delta$ distribution | |
| $\delta E$ | small variation of $E$ | $W\,m^{-2}$ |
| $\delta t$ | small variation of $t$ | s |
| $\Delta T$ | pulse-related temperature increment, defined in Eq. (7) | K |
| $\Delta t$ | duration of relevant pulse-related effects | s |
| $\varepsilon$ | emissivity | |
| $\varepsilon_t$ | total linear thermal and volumic expansion | |
| $\theta$ | Laplace transform of $T$ | K |
| $\Pi(\ldots)$ | rectangle function (equal to 1 in $[-1/2, 1/2]$, to 0 elsewhere) | |
| $\rho$ | density | $kg\,m^{-3}$ |
| $\sigma$ | Stefan–Boltzmann constant | $W\,m^{-2}\,K^{-4}$ |
| $\tau$ | dimensionless time $t/t_c$ | |
| $\tilde{\tau}$ | dimensionless time $(t - t_0)/t_c$ | |
| $\chi$ | dimensionless position $x/L$ | |

*Subscripts*

| | |
|---|---|
| II | solution of Eq. (2) |
| III | solution of Eq. (3) |
| VI | solution of Eq. (6) |
| in | input to the numerical simulation |
| out | output from the numerical simulation |

*Superscripts*

| | |
|---|---|
| $^\circ$ | derivative in respect to $t$ |
| $'$ | derivative in respect to $x$ |

phase-dependent thermophysical properties can be employed in order to seek more accurate results.[2]

Because these data are seldom available for a specific steel grade, it is useful to evaluate which property is more influent upon the quench process, and therefore is worth to be more accurately assessed. If the Biot number[3] of the quench process is small (lower than 0.1), the temperature differences inside the steel component are negligible and the cooling curve depends mainly upon the boundary conditions and the specific heat capacity. On the contrary, if the same number is large, relevant temperature differences occur inside the component and the heat flux is mainly determined by the steel's thermal diffusivity [6,7]. A problem characterized by a small Biot number may not actually require a finite-elements model, because it can be satisfyingly analyzed by a simple lumped capacitance model and it can be controlled by measuring the surface temperature, the as-quenched microstructure being sensibly homogeneous in the volume. The opposite considerations can hold if the Biot number is large. Therefore, the thermal diffusivity is usually the more influent thermophysical property in those quench processes that can most usefully be analyzed by finite-element thermo-metallurgical models.

Moreover, in any effective steel quenching process a large fraction of the component's volume necessarily consists of metastable undercooled austenite during most of the process duration. Thus, the thermal diffusivity of the metastable (undercooled) austenite is particularly relevant for the numerical simulation of the steel quench.

Yet, the standard thermal diffusivity measurement methods, and particularly the flash method [8], require the specimen to be initially held at constant temperature and in thermal equilibrium with the specimen holder and the testing ambient (furnace).

As it regards the measurement of undercooled austenite, depending upon the kinetic of the phase transformation (i.e. upon

[2] Whereas only the thermophysical properties are discussed here, the kinetic model of the metallurgical transformations may have an even deeper influence upon the precision of a thermo-metallurgical simulation.

[3] Defined as $Bi = h \cdot L/k$, being $h$ the surface heat transfer coefficient, $k$ the thermal conductivity, and $L$ a representative linear dimension of the body.

the steel's hardenability [1]), upon the furnace's control systems and upon the desired measurement temperature, it can be possible to austenitize a steel specimen in the measurement furnace itself and then to quench it to the measurement temperature, but it may be very difficult or impossible to achieve the required initial equilibrium condition while avoiding transformation.

Therefore, the thermal diffusivity of the undercooled austenite has been measured by a non-standard laser-flash method, which was derived by the standard one by dropping the prior equilibrium requirement.

## Experimental

The alloyed, medium-carbon, ISO 1.2738 steel grade[4] [9] was chosen because it is usually employed for the production of very large pre-hardened blooms [10,11]. The heat treatment of these blooms is characterized by a large Biot number and is relevant to control mechanical properties; thus, finite-element analyses need to be performed for die design purposes. Moreover, this steel shows a very high hardenability, that allowed to effectively quench the samples by cooling them inside the measurement furnace, and a large separation between the pearlitic and bainitic transformation temperature ranges, that allows to retain a fully austenitic structure for more than one day at temperatures between about 720 and 770 K (Fig. 1, [12–15]).

A steel sample disk, having a diameter of $9.9 \cdot 10^{-3} \pm 10^{-5}$ m and a thickness $L$ of $2.47 \cdot 10^{-3} \pm 10^{-5}$ m, was obtained from a commercial bloom (Table 1) and austenitized at 1133 K for 1/2 hour.[5] Thereafter, the disk was allowed to cool to 755 K, held at this temperature for about one hour, and finally allowed to cool to room temperature (Fig. 1). Flash measurements were performed at the austenitizing temperature (after the completion of the austenitization), during the cooling stage between 1133 and 755 K, and during the 755 K holding stage (after the end of the furnace transient).

The thermal cycle and the flash measurements were performed inside a vacuum furnace; during the constant-temperature stages the sample-holder's temperature was closed-loop controlled, whereas during the cooling stages the sample was cooled by the natural irradiation, i.e. the heat from the sample itself, from the sample-holder and from other furnace parts was dissipated to the water-cooled external furnace walls (trough intermediate thin metal screens).

The flash measurements were performed by laser pulses, whose duration was 600 μs. The pulse instant was accurately recorded by a photodiode. The time-temperature curves (thermographs) were acquired at 400 Hz from a thermocouple welded to the sample, with the recording beginning 0.5 s before the laser pulse and lasting 2.5 s. A digital filter was employed to remove from the thermographs some disturbances. During the holding stages, measurements were performed both by keeping the heating system on, or by switching it off about 1 s before the laser pulse and for the duration of the measurement (in order to reduce the intensity of the disturbances).

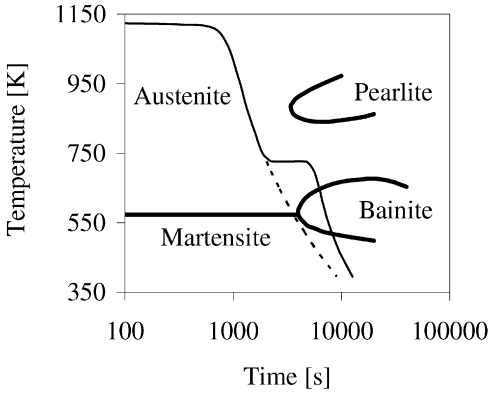


Fig. 1. Approximate sketch of the sample's actual cooling curve and of the corresponding curve obtained by neglecting the 755 K holding stage (dashed), superimposed to the steel's CCT (Continuous Cooling Transformation) diagram.

Table 1
Chemical composition of the employed alloy steel

| C | Cr | Mn | Ni | Mo | Si | P | S |
|---|---|---|---|---|---|---|---|
| 0.388 | 2.132 | 1.492 | 0.969 | 0.192 | 0.214 | 0.009 | 0.007 |

The precision of the measurement apparatus was verified by performing two successive series of standard flash measurements [8] on an Armco iron sample, with the same data acquisition and filtering procedures. The difference between the measured diffusivity values and the literature data [17] in the temperature range from 297 to 1004 K is lower than 5%, that is the repeatability of standard laser flash measurements [8]; at higher temperatures the same difference is larger, and therefore the experimental apparatus is probably less precise, although the comparison is less certain due to the proximity of the magnetic and phase transitions (Fig. 2).

The sample's post-cooling microstructure, assessed by optical metallography after a Nital etch [18], was martensite. Moreover, the previous austenitic grain boundaries were evidenced by the Bechet–Beaujard etch [19,20]; the mean austenitic grain size, measured by using the three-circle intersection procedure [21], was 12 μm.

Whereas in the reported sample, and in other ones tested with similar schedules, the pearlitic and bainitic transformations were avoided, one attempt to perform standard flash measurements while holding another sample at 923 K resulted in a partially pearlitic final microstructure, implying that this sample was transforming before and during these measurements; therefore they were discarded.

## Analytical model

Typical thermographs obtained from standard and non-standard measurements are compared in Fig. 3. Whereas the

[4] Similar to the AISI P20 grade, with a 1 wt% nickel addition.

[5] The sample's metallurgical condition prior to the austenitization, some standard flash measurements performed before the austenitization, and other standard and non-standard measurements performed upon other samples of the same steel, were previously reported [16].

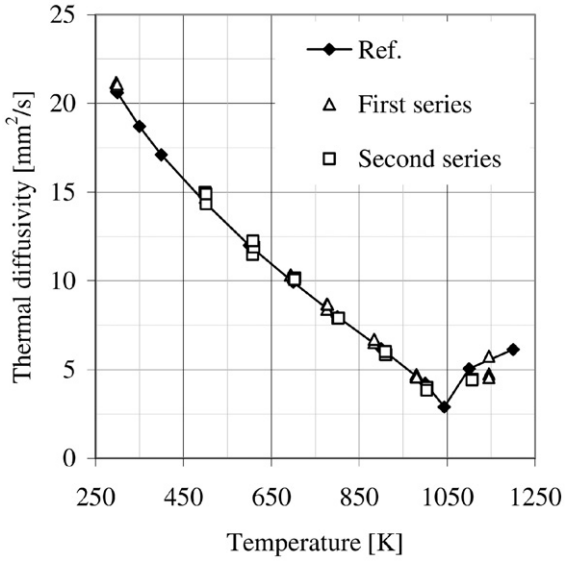


Fig. 2. Thermal diffusivity of Armco iron. Literature values and standard laser flash measurements performed with the present apparatus.

former (Fig. 3(a)) is close to the standard analytical model originally introduced by Parker et al. [22], the latter (Fig. 3(b)) is significantly different and may be described qualitatively as the superposition of a contribution due to the energy pulse upon a base curve pertaining to the sample cooling process. Although both these contributions arise from transient phenomena, the radiative heat exchange between the sample and the furnace leads to a comparatively slow cooling of the sample (e.g.: on a time scale of the order of $10^3$–$10^4$ s in the present experiment, mainly determined by the furnace), whereas the observable effects of the laser pulse vanish in a comparatively very short time interval (e.g.: of the order of 1 s in the present experiment). Moreover, because the purpose of the measurements is to determine the sample's diffusivity from the effects of the laser pulse, the radiative heat exchange can be regarded essentially as a disturbance. Therefore, it is sufficient to adopt a model of the radiative heat exchange that can satisfyingly fit the radiative cooling curve for a time interval safely longer than the duration of the relevant laser pulse effects, but still very short in respect to the time scale of the sample cooling process. One such model is chosen by assuming constant diffusivity and conductivity and by using a constant-heat-flux boundary condition. The experiments and the non-linear numerical simulations described in the following chapters show that this approximation is sufficient for the above mentioned purpose. Moreover, this choice does not require any knowledge of the furnace characteristics, and it allows a closed form analytical solution, that is derived hereafter.

It is assumed that the sample is a slab of thickness $L$, thermal diffusivity $\alpha$ and thermal conductivity $k$, and that it is cooling from an initial temperature $T_0$ due to a constant outgoing surface heat flux $E$ at both its surfaces, both before and after an ideal pulse of surface energy $q$ is absorbed upon the first surface. This one-dimensional model is described by the following partial differential equation and boundary conditions:

$$\begin{cases} \dot{T} = \alpha \cdot T'', & x \in [0, L] \\ -k \cdot T' = q \cdot \delta(t - t_0) - E, & x = 0,\ t \geqslant 0 \\ -k \cdot T' = E, & x = L,\ t \geqslant 0 \\ T = T_0, & t \leqslant 0 \end{cases} \tag{1}$$

where $T$ is the temperature, $t$ is the time, $x$ is the position inside the sample (comprised between 0 and $L$), a superscript dot and an apex indicate the derivation in respect to $t$ and $x$ respectively, $\delta(t)$ is the Dirac distribution, and $t_0$ is the (positive) instant when the energy pulse is absorbed.

It can be demonstrated that, if the functions $T_{\mathrm{II}}$ and $T_{\mathrm{III}}$ satisfy the following sets of equations:

$$\begin{cases} \dot{T}_{\mathrm{II}} = \alpha \cdot T''_{\mathrm{II}}, & x \in [0, L] \\ -k \cdot T'_{\mathrm{II}} = -E, & x = 0 \\ -k \cdot T'_{\mathrm{II}} = E, & x = L \\ T_{\mathrm{II}} = T_0, & t = 0 \end{cases} \tag{2}$$

$$\begin{cases} \dot{T}_{\mathrm{III}} = \alpha \cdot T''_{\mathrm{III}}, & x \in [0, L] \\ -k \cdot T'_{\mathrm{III}} = q \cdot \delta(t), & x = 0 \\ -k \cdot T'_{\mathrm{III}} = 0, & x = L \\ T_{\mathrm{III}} = 0, & t \leqslant 0 \end{cases} \tag{3}$$

then, the function $T$ defined by:

$$T(x, t) = T_{\mathrm{III}}(x, t - t_0) + T_{\mathrm{II}}(x, t) \tag{4}$$

satisfies Eq. (1). Thus, the thermal transient $T_{\mathrm{II}}$ satisfying Eq. (2) can be regarded as the above-mentioned slow cooling contribution to the sample thermal history $T(x, t)$, whereas the thermal transient $T_{\mathrm{III}}$ (satisfying Eq. (3) and translated in time) can be regarded as the above-mentioned pulse-related contribution.[6]

The solution $T_{\mathrm{II}}$ of Eq. (2), re-arranged from the literature [23], is:

$$T_{\mathrm{II}}(t, x) = T_0 + z(x) - B \cdot t + B \cdot t_c \cdot f_{\mathrm{II}}\left(\frac{t}{t_c}, \frac{x}{L}\right)$$

with

$$\begin{cases} z(x) = Z \cdot \left\{\frac{1}{3} - \left(\frac{2 \cdot x}{L} - 1\right)^2\right\} \\ Z = B \cdot t_c \cdot \pi^2/8 \\ B = \frac{2 \cdot E \cdot \alpha}{k \cdot L} \\ t_c = \frac{L^2}{\pi^2 \cdot \alpha} \\ f_{\mathrm{II}}(\tau, \chi) = \frac{1}{2} \cdot \sum_{n=1}^{\infty} \frac{(-1)^n}{n^2} \cdot \exp\left(-4 \cdot \tau \cdot n^2\right) \\ \quad \cdot \cos\left(n \cdot \pi \cdot (2 \cdot \chi - 1)\right) \end{cases} \tag{5}$$

where $t_c$ is the sample's characteristic time. After a brief transient described by the vanishing term $f_{\mathrm{II}}$, this solution predicts a constant cooling rate $B$[7] and a constant parabolic tem-

[6] It can be demonstrated that if the sample cooling was modeled by a radiative or convective boundary condition the two contributions would not results rigorously additive.

[7] Because of this result, and because it is intended to describe only a relatively short time interval, the present model can also be regarded as a local linearization of the overall cooling curve.

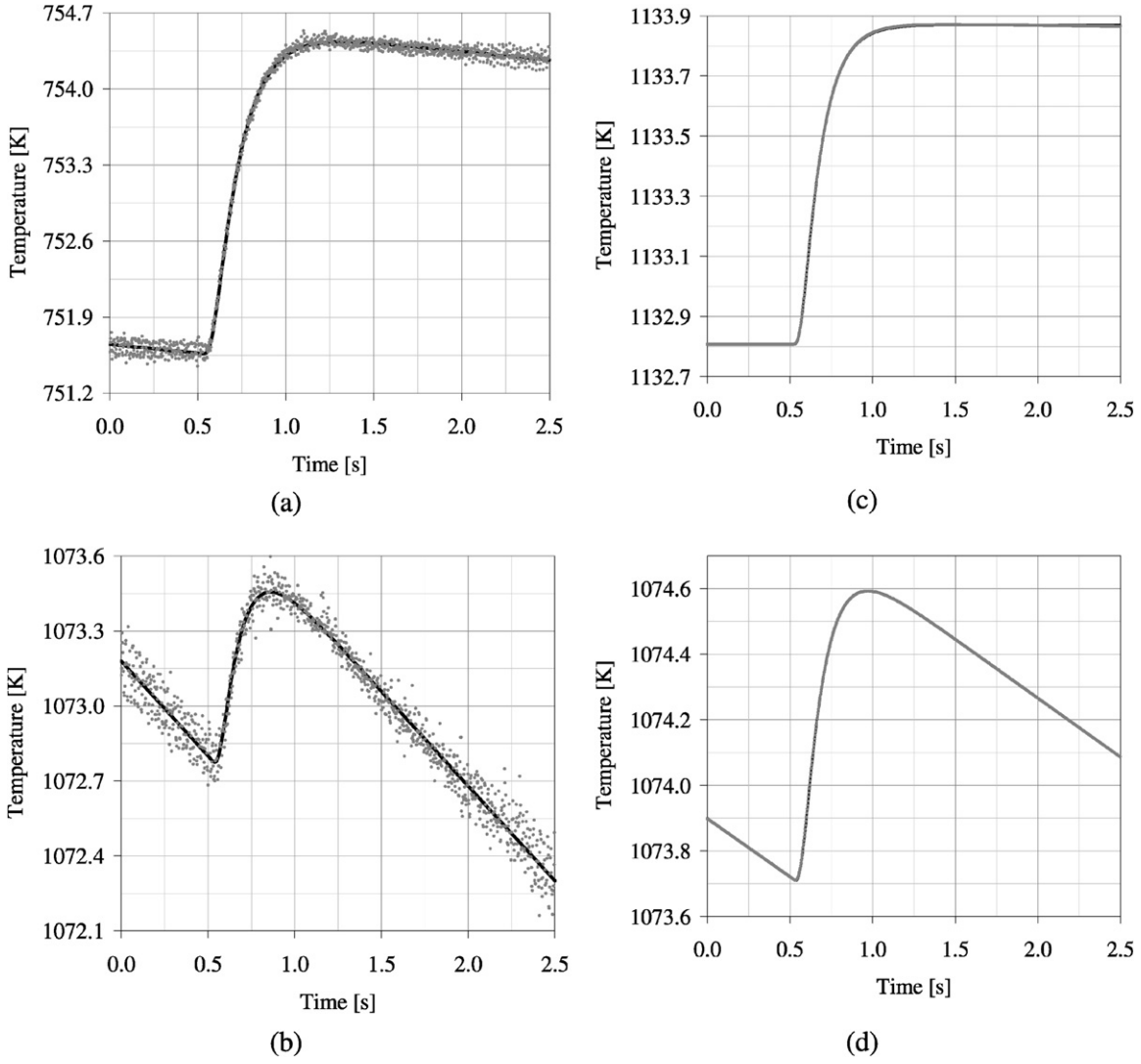


Fig. 3. Time-temperature thermographs. Standard flash measurement (a). Non-standard flash measurement performed during an uninterrupted sample cooling process (b). Simulated standard (c) and non-standard (d) flash measurements. Acquired or simulated time-temperature points and interpolating curves.

perature gradient inside the sample, whose total magnitude is $z(b/2) - z(0) = Z$.

The pulse transient described by Eq. (3) is physically similar to the original Parker et al. model:

$$\lim_{\delta\to 0}\begin{Bmatrix} \dot{T}_{\mathrm{VI}} = \alpha\cdot T''_{\mathrm{VI}}, & x\in[0,L] \\ -k\cdot T'_{\mathrm{VI}} = 0, & x = 0 \\ -k\cdot T'_{\mathrm{VI}} = 0, & x = L \\ T_{\mathrm{VI}} = \begin{Bmatrix} q/(\rho\cdot c_p\cdot\delta), & x\in[0,\delta] \\ 0, & x\in(\delta,L] \end{Bmatrix}, & t = 0 \end{Bmatrix} \tag{6}$$

provided that this latter model is arbitrarily extended by the constant temperature $T_0$ when $t < 0$. Nevertheless, whereas in the proposed model, and therefore in Eq. (3), the pulse surface energy $q$ appears in a boundary condition, in the Parker et al. model (Eq. (6)) it appears in the initial condition. Therefore, contrary to the solution of Eq. (3), the original Parker et al. solution cannot be rigorously translated in time and added to the solution of Eq. (2).

A closed-form solution $T_{\mathrm{III}}$ of Eq. (3) is derived in the appendix and, in the point $x = L$, it is:

$$T_{\mathrm{III}}(t,x) = \Delta T\cdot f_{\mathrm{III}}\left(\frac{t}{t_c},\frac{x}{L}\right)$$

with

$$\begin{cases} \Delta T = \frac{q\cdot\alpha}{k\cdot L} = \frac{q\cdot S}{C} \\ f_{\mathrm{III}}(\tau,1) = 0, \quad \tau\leqslant 0 \\ f_{\mathrm{III}}(\tau,1) = 2\cdot\sqrt{\frac{\pi}{\tau}}\cdot\sum_{n=0}^{\infty}\exp\left(-\frac{\pi^2}{\tau}\cdot\left(n+\frac{1}{2}\right)^2\right), \quad \tau > 0 \end{cases} \tag{7}$$

where $\Delta T$ is the asymptotic temperature increase due to the pulse energy and can also be expressed by using the sample's total heat capacity $C$ and section area $S$.

For comparison, the extended Parker et al. solution, in the same point, is:

$$T_{\mathrm{VI}}(t,x) = \Delta T \cdot f_{\mathrm{VI}}\left(\frac{t}{t_c}, \frac{x}{L}\right)$$

with

$$\begin{cases} f_{\mathrm{VI}}(\tau, 1) = 0, & \tau \leqslant 0 \\ f_{\mathrm{VI}}(\tau, 1) = 1 + 2 \cdot \sum_{n=1}^{\infty} (-1)^n \cdot \exp\left(-\mathrm{n}^2 \cdot \tau\right), & \tau > 0 \end{cases} \tag{8}$$

Although it has not been demonstrated whether Eqs. (3) and (6) are rigorously equivalent for $t > 0$, their respective solutions $T_{\mathrm{III}}$ and $T_{\mathrm{VI}}$ (Eqs. (7) and (8)) are numerically equal in the point $x = L$ and in the time interval relevant to the present work;[8] therefore they will be used indifferently in these limits.

By introducing Eqs. (5) and (7) (or (8)) into Eq. (4), the complete solution of the proposed analytical model (described by Eq. (1)) is:

$$T(t,x) = T_0 + z(x) - B \cdot t + \Delta T \cdot f_{\mathrm{III–VI}}\left(\frac{t - t_0}{t_c}, \frac{x}{L}\right) + B \cdot t_c \cdot f_{\mathrm{II}}\left(\frac{t}{t_c}, \frac{x}{L}\right) \tag{9}$$

If the initial cooling transient term $f_{\mathrm{II}}$ can be neglected, the initial condition $T = T_0$ can be imposed at, and the time $t$ can be measured from, any arbitrary starting instant, e.g.: shortly before the laser pulse instant; if moreover only the point $x = L$ is of interest, the solution reduces to the sum of a linear cooling term and of the standard Parker et al. curve, i.e.:

$$T(t,L) \approx A - B \cdot t + \Delta T \cdot f_{\mathrm{III–VI}}\left(\frac{t - t_0}{t_c}, 1\right)$$

with

$$A = T_0 + z(L) \tag{10}$$

Furthermore, by integrating Eq. (9) in respect to $x$, it can be demonstrated (Appendix A) that the spatial average sample temperature $\overline{T}$ is rigorously equal to:

$$\overline{T}(t) = \frac{1}{L} \cdot \int_0^L T(t,x)\,\mathrm{d}x = T_0 - B \cdot t + \Delta T \cdot u(t - t_0) \tag{11}$$

where $u(t)$ is the unitary step function. The relevant measurement temperature $\overline{\overline{T}}$ can be defined as the average sample temperature in a relevant time interval $\Delta t$ during which the pulse transient sensibly affects the sample temperature and is actually measured; i.e.:

$$\overline{\overline{T}} = \frac{1}{\Delta t} \cdot \int_{t_0}^{t_0 + \Delta t} \overline{T}(t)\,\mathrm{d}t = T_0 - B \cdot (t_0 + \Delta t/2) + \Delta T. \tag{12}$$

By calculating $z(L)$ from the definition of $z(x)$ given in Eq. (5) and by introducing $A$ as defined in Eq. (10), it results:

$$\overline{\overline{T}} = A + \frac{\pi^2}{12} \cdot B \cdot t_c - B \cdot (t_0 + \Delta t/2) + \Delta T \tag{13}$$

[8] Upon calculating the two function with a 64 bit precision, for $\tau$ comprised in the 0 to 10 range, the maximum absolute difference is lower than $5 \cdot 10^{-16}$.

Therefore, if the laser pulse instant $t_0$ and the sample thickness $L$ are known, the quantities $A$, $B$, $\Delta T$ and $t_c$ can be obtained by fitting the experimental data upon the curve given in Eq. (10) in a time interval conveniently extended before and after the pulse instant (although necessarily short in respect to the overall radiative cooling process), and the thermal diffusivity $\alpha$ and the corresponding relevant sample temperature $\overline{\overline{T}}$ can be calculated, by using the definition of $t_c$ (given in Eq. (5)), and Eq. (13), respectively, and by choosing a relevant $\Delta t$ value.

## Experimental data reduction

Each thermograph was fitted with Eq. (10), using the minimum least square method and considering all the measured data (Fig. 3). The minimum searching procedure of Lagarias et al. [24], as implemented in a general-purpose computation code [25], was employed to find the minimum of the least-square residual as a function of the fitting parameters $A$, $B$, $\Delta T$ and $t_c$.

This procedure requires a first estimation of the minimum, that, for each thermograph, was calculated as follows. First estimates of $A$ and $B$ were obtained from the linear least-square interpolation of the initial part of the thermograph, prior to the laser pulse. First estimates of $\Delta T$ and $t_c$ were obtained by applying the standard half-time method [8] upon the difference between the actual thermograph and the first estimate $A - B \cdot t$ of the linear cooling contribution.

For the sake of homogeneity, this data reduction procedure was applied also to the standard flash measurements; in these cases it yields a cooling rate $B$ close to zero and therefore becomes almost equivalent to fitting the curve with the standard Parker et al. function. Moreover, the cooling rate $B$ can be assumed as an index of how much a specific measurement deviates from the standard model.

The measurement temperatures $\overline{\overline{T}}$ were calculated by choosing $\Delta t = 5 \cdot t_c$, which corresponds to an almost 99% rise of the Parker et al. curve (Fig. 4(a)).

The calculated thermal diffusivities $\alpha$ and measurement temperatures $\overline{\overline{T}}$ are reported in Table 2, with the respective cooling rates $B$.

Moreover, the ratio of the sample's emissivity $\varepsilon$ and total heat capacity $C$ was estimated, for each laser flash measurement, by comparing the absorbed pulse energy $Q_a$ (equal to the product of $q$ and $S$) with the nominal incident pulse energy $Q_i$ (known from the laser apparatus) and by recalling from Eq. (7) that $\Delta T = q \cdot S/C$, i.e. by using the following equation:

$$\varepsilon = \frac{Q_a}{Q_i} = \frac{q \cdot S}{Q_i} \approx \frac{C \cdot \Delta T}{Q_i} \tag{14}$$

These $\varepsilon/C$ ratios are also reported in Table 2, as well as other validity or precision parameters discussed thereafter.

## Numerical verifications

A numerical simulations of a whole sample time-temperature history was performed as an aid to evaluate the uncertainties deriving from some simplifying hypotheses employed in

Table 2
Experimental laser flash measurements

| Stage | Heating | $\overline{\overline{T}}$ K | $\alpha$ $10^{-6}$ m$^2$ s$^{-1}$ | $B$ K s$^{-1}$ | $B \cdot t_c$ K | $B \cdot \Delta t$ K | $Z$ K | $\Delta T$ K | $\varepsilon/C$ K J$^{-1}$ | $D$ % | $R$ K | $\Delta T/R$ – |
|---|---|---|---|---|---|---|---|---|---|---|---|---|
| 1133 K holding | off | 1131 | 5.67 | 0.50 | 0.05 | 0.27 | 0.07 | 1.02 | 0.10 | – | 0.10 | 11 |
| | | 1130 | 5.44 | 0.50 | 0.06 | 0.28 | 0.07 | 1.05 | 0.11 | – | 0.09 | 11 |
| | on | 1135 | 5.41 | 0.02 | 0.00 | 0.01 | 0.00 | 0.95 | 0.09 | – | 0.11 | 8 |
| | | 1133 | 5.29 | −0.07 | −0.01 | −0.04 | −0.01 | 0.86 | 0.09 | – | 0.11 | 8 |
| | | 1135 | 5.39 | 0.11 | 0.01 | 0.06 | 0.02 | 1.10 | 0.11 | – | 0.10 | 11 |
| Continuous cooling | off | 1121 | 5.36 | 0.67 | 0.08 | 0.39 | 0.10 | 1.00 | 0.10 | 2.42 | 0.08 | 13 |
| | | 1075 | 5.40 | 0.76 | 0.09 | 0.43 | 0.11 | 1.02 | 0.10 | 2.22 | 0.06 | 17 |
| | | 1026 | 5.01 | 0.66 | 0.08 | 0.41 | 0.10 | 1.07 | 0.11 | 2.09 | 0.08 | 14 |
| | | 977 | 4.97 | 0.56 | 0.07 | 0.35 | 0.09 | 1.11 | 0.11 | 1.94 | 0.09 | 12 |
| | | 923 | 4.77 | 0.44 | 0.06 | 0.29 | 0.07 | 1.15 | 0.12 | 1.75 | 0.10 | 12 |
| | | 886 | 4.67 | 0.39 | 0.05 | 0.26 | 0.06 | 1.21 | 0.12 | 1.68 | 0.08 | 15 |
| | | 834 | 4.47 | 0.31 | 0.04 | 0.21 | 0.05 | 1.26 | 0.13 | 1.52 | 0.05 | 23 |
| | | 768 | 4.39 | 0.25 | 0.04 | 0.18 | 0.04 | 1.35 | 0.14 | 1.36 | 0.06 | 24 |
| | | 754 | 4.25 | 0.22 | 0.03 | 0.16 | 0.04 | 1.37 | 0.14 | 1.33 | 0.03 | 41 |
| | | 722 | 4.15 | 0.20 | 0.03 | 0.15 | 0.04 | 1.42 | 0.14 | 1.25 | 0.06 | 25 |
| 755 K holding | off | 757 | 4.27 | 0.20 | 0.03 | 0.15 | 0.04 | 3.12 | n.a. | – | 0.04 | 73 |
| | | 756 | 4.23 | 0.24 | 0.04 | 0.18 | 0.04 | 3.15 | n.a. | – | 0.05 | 67 |
| | | 750 | 4.24 | 0.23 | 0.03 | 0.17 | 0.04 | 3.17 | n.a. | – | 0.04 | 76 |
| | on | 754 | 4.31 | 0.12 | 0.02 | 0.09 | 0.02 | 2.97 | n.a. | – | 0.05 | 55 |
| | | 755 | 4.19 | 0.16 | 0.02 | 0.12 | 0.03 | 3.02 | n.a. | – | 0.05 | 63 |
| | | 757 | 4.27 | 0.16 | 0.02 | 0.12 | 0.03 | 3.08 | n.a. | – | 0.06 | 55 |

Holding or cooling stage, furnace heating system status, average temperature $\overline{\overline{T}}$, thermal diffusivity $\alpha$, cooling rate $B$, temperature coefficient of the cooling process initial transient $B \cdot t_c$, temporal and spatial temperature differences $B \cdot \Delta t$ and $Z$, pulse-related temperature increase $\Delta T$, estimated ratio of emissivity and total heat capacity $\varepsilon/C$, heat flux variation parameter $D$, thermograph interpolation root mean square residual $R$, effective signal-to-noise ratio $\Delta T/R$.

the above described analytical model. Therefore, in the numerical model, the diffusivity and the specific heat capacity are considered functions of the temperature, the laser pulses are modeled with rectangle functions, and the radiative heat exchange between the sample and the furnace is modeled with the Stefan–Boltzmann law by considering the sample as a gray-body and the furnace interior as a blackbody, and by noting that the view factor is 1. The resulting one-dimensional model is:

$$\begin{cases} \rho \cdot c_p \cdot \dot{T} = \frac{\partial}{\partial x}(\alpha \cdot \rho \cdot c_p \cdot T'), & x \in [0, L] \\ -\alpha \cdot \rho \cdot c_p \cdot T' = P - \varepsilon \cdot \sigma \cdot (T^4 - T_f^4), & x = 0,\ t \geqslant 0 \\ -\alpha \cdot \rho \cdot c_p \cdot T' = \varepsilon \cdot \sigma \cdot (T^4 - T_f^4), & x = L,\ t \geqslant 0 \\ T = T_0, & t \geqslant 0 \end{cases} \tag{15}$$

with

$$P = \frac{\varepsilon \cdot Q_i}{S \cdot t_p} \cdot \sum_n \Pi\left(\frac{t - t_{0n}}{t_p}\right)$$

where $\sigma$ is the Stefan–Boltzmann constant,[9] $P$ is the instantaneous adsorbed surface power due to the laser pulses, $\Pi$ is the rectangle function, $t_p$ is the duration of each laser pulse (equal to 0.6 ms), $t_{0n}$ is the $n$th laser pulse instant, and $T_f(t)$ is the furnace cooling curve between 1133 and 755 K.[10]

[9] Equal to $5.6704 \cdot 10^{-8}$ W m$^{-2}$ K$^{-4}$.

[10] Measured while performing a thermal cycle similar to the experimental one, with a thermocouple instead of the sample.

The specific heat capacity was obtained from the literature, by considering unalloyed austenite [26]. Because the simulation does not take account of the thermal expansion, the density was considered constant and equal to 7800 kg m$^{-3}$. The diffusivity was obtained from the overall result of the present experiments (Eq. (25) below). The emissivity was estimated as the average (equal to 0.100) of the values calculated from each laser flash experiment; these values were obtained from the above-mentioned $\varepsilon/C$ ratios (Table 2) by neglecting the wavelength dependency and by using the sample dimensions and the above-mentioned density and specific heat capacity to calculate $C$.

The model was solved by using a numerical method [27] implemented in a general-purpose computation code [25]. The sample thickness was discretized into 50 equal elements. The simulation time steps were smaller than 0.12 ms during each laser pulse and smaller than 1.25 ms for a duration of 2 s after each laser pulse. A simulated thermograph, with the same sampling period and duration (before and after the laser pulse instant) employed in the actual measurements, was calculated for each simulated measurement. The pulse instants $t_{0n}$ were chosen to perform 3 simulated (standard) measurements at the initial temperature, a series of 8 simulated measurements during the cooling process, and 3 simulated measurements at the end of the same process.

One standard and one non-standard simulated thermographs are reported in Fig. 3(c) and Fig. 3(d), respectively.

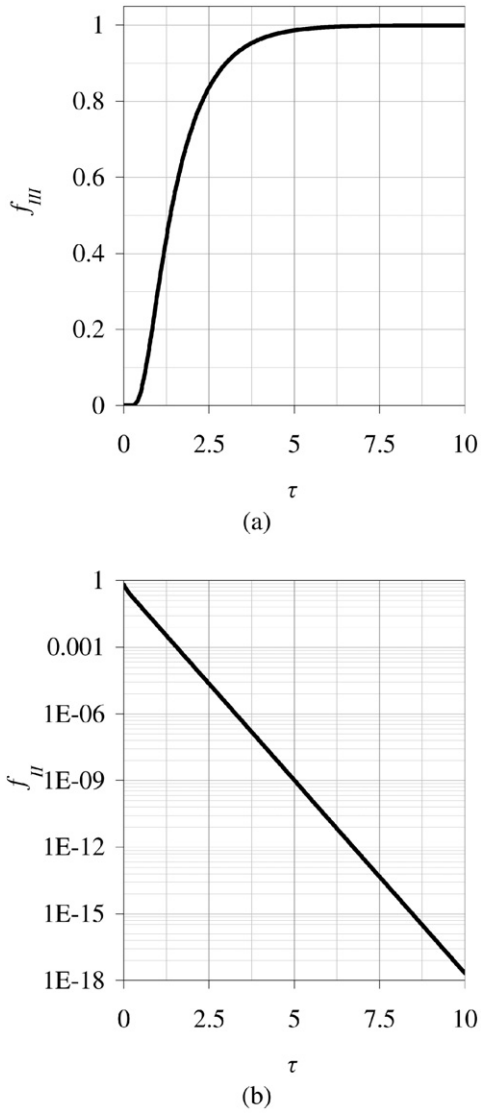


Fig. 4. The non-dimensional functions $f_{\mathrm{III–VI}}(\tau, 1)$ and $f_{\mathrm{II}}(\tau, 1)$ employed in the analytical model (a and b).

## Limitations and uncertainties

Limitations to the validity of the proposed data reduction method arise from the differences between the experiment and the proposed analytical model.

This model, as the original Parker et al. model, assumes an ideal (instantaneous and uniform) energy pulse and disregards the eventual heat flux from the sample's side (cylindrical) surface, even if these two assumptions were later dropped in more refined models [28–30]. Therefore, the same limitations and uncertainties of the original Parker et al. model, deriving from these two assumptions, apply also to the present model.

The contribution due to the initial transient of the continuous cooling process, represented by the term $B \cdot t_c \cdot f_{\mathrm{II}}$ in Eq. (9), can be estimated from the calculated cooling rate $B$ and characteristic time $t_c$ and from the numerical values of the function $f_{\mathrm{II}}$. In the reported flash measurements, the $B \cdot t_c$ temperature coefficient was always lower than 0.1 K (Table 2). Furthermore, $f_{\mathrm{II}}(2, 1)$ is lower than $10^{-3}$ and $f_{\mathrm{II}}(5, 1)$ is lower than $10^{-8}$ (Fig. 4(b)). Therefore, if a time interval only a few times longer than $t_c$ is allowed between the start of the overall sample cooling process and the flash measurement(s), no significant error arises from having neglected this contribution in the numerical interpolation. This condition is safely achieved.

Both standard and non-standard flash measurements must be referred to an averaged sample temperature, because necessarily different temperatures occur inside the sample at different times and positions. Whereas in the standard measurements these temperature differences arise from the pulse transient only, in the proposed non-standard measurements they arise also from the overall sample cooling process, both in time, i.e. $B \cdot \Delta t$, and in space, i.e. $Z$. In the present non-standard measurements, the former were lower or comparable (at the highest temperatures), and the latter always much lower, than the temperature increase $\Delta T$ due to the energy pulse (Table 2). Moreover, the temperature differences arising from the cooling process are mostly opposite to those due to the pulse transient and thus the former ones partially cancel the latter. Therefore the temperature-related uncertainty wasn't significantly increased in the non-standard measurements, in respect to standard ones.

A more important uncertainty arises in the proposed model from the constant surface heat flux boundary condition adopted in Eq. (1). Because the sample's cooling physically arises from a radiative heat transfer process, such a boundary condition is acceptable only if the surface heat flux variation $\delta E$, occurring during a time interval $\delta t$ comparable to the duration of a flash measure, is small in respect to the surface heat flux $E$ itself. Indicative values of $|\delta E|$, $|E|$ and $|\delta E/E|$ calculated from the results of the numerical simulation are reported in Table 3: $|E|$ was calculated as the integral mean heat flux in each data acquisition period, and $|\delta E|$ as the difference between the maximum and minimum instantaneous heat flux values in the same periods. In the simulated standard measurements $|\delta E/E|$ is large, because $|E|$ is initially zero (in the first simulated measurement) or low and then increases due to the pulse-related temperature rise, but in these cases $|E|$ itself does not significantly influence the test because it is always low in respect to the sample's thermal capacity and to the duration of the measurement. On the contrary, in the simulated measurements performed during the cooling process, $|E|$ is sufficiently large to yield a clear cooling contribution in the thermograph, but $|\delta E/E|$ is small (of the order of 1% in most cases), because the mean sample temperature is substantially higher than the mean furnace temperature, and thus the temperature variations are comparatively low. Therefore, the constant heat flux boundary condition is a fair approximation in most cases.

Furthermore, it may be possible to estimate $|\delta E/E|$ during the cooling stage without performing a numerical simulation, by considering the overall (experimental) sample cooling curve only, even if the temperature of the furnace components in view of the sample is not known. To this purpose, if the Biot number associated with the overall cooling process is small (e.g. smaller than 0.1), as a first approximation and as it regards this overall cooling process only, a lumped capacitance model can be

Table 3
Simulated laser flash measurements

| Stage | $\overline{\overline{T}}_{out}$ K | $\alpha_{out}$ $mm^2\,s^{-1}$ | $\lvert\alpha_{in}-\alpha_{out}\rvert$ $mm^2\,s^{-1}$ | $\lvert(\alpha_{out}/\alpha_{in})-1\rvert$ % | $\delta E$ $W\,m^{-2}$ | $E$ $W\,m^{-2}$ | $\delta E/E$ – | $B_{out}$ $K\,s^{-1}$ | $\Delta T_{out}$ K | $R_{out}$ mK | $\Delta T_{out}/R_{out}$ – |
|---|---|---|---|---|---|---|---|---|---|---|---|
| Holding | 1134 | 5.47 | 0.0287 | 0.527 | 34 | 24 | 1.452 | 0.00 | 1.06 | 1.87 | 568 |
| | 1135 | 5.45 | 0.0019 | 0.034 | 36 | 45 | 0.787 | 0.01 | 1.07 | 0.72 | 1489 |
| | 1135 | 5.45 | 0.0024 | 0.043 | 35 | 58 | 0.601 | 0.01 | 1.07 | 0.71 | 1497 |
| Continuous cooling | 1122 | 5.40 | 0.0015 | 0.029 | 59 | 1330 | 0.044 | 0.23 | 1.07 | 0.79 | 1358 |
| | 1075 | 5.26 | 0.0003 | 0.005 | 32 | 2101 | 0.015 | 0.36 | 1.08 | 0.68 | 1592 |
| | 1024 | 5.10 | 0.0002 | 0.004 | 25 | 2048 | 0.012 | 0.35 | 1.10 | 0.59 | 1856 |
| | 972 | 4.93 | 0.0018 | 0.037 | 21 | 1794 | 0.012 | 0.31 | 1.11 | 0.57 | 1967 |
| | 917 | 4.76 | 0.0021 | 0.044 | 18 | 1482 | 0.012 | 0.26 | 1.13 | 0.54 | 2073 |
| | 878 | 4.64 | 0.0025 | 0.054 | 16 | 1271 | 0.013 | 0.23 | 1.14 | 0.51 | 2240 |
| | 830 | 4.49 | 0.0012 | 0.027 | 16 | 642 | 0.025 | 0.12 | 1.16 | 0.55 | 2117 |
| | 800 | 4.40 | 0.0010 | 0.024 | 13 | 188 | 0.068 | 0.03 | 1.16 | 0.47 | 2478 |
| Holding | 779 | 4.33 | 0.0027 | 0.062 | 12 | 17 | 0.739 | 0.00 | 1.17 | 0.47 | 2469 |
| | 779 | 4.33 | 0.0019 | 0.045 | 12 | 25 | 0.496 | 0.00 | 1.17 | 0.49 | 2404 |
| | 780 | 4.34 | 0.0018 | 0.041 | 12 | 40 | 0.316 | 0.01 | 1.17 | 0.49 | 2390 |

Input values (in) and values calculated from the simulated thermographs (out). Holding or cooling stage, average temperature $\overline{\overline{T}}_{out}$, output thermal diffusivities $\alpha_{out}$ and differences between input and output values $\alpha_{in}$ and $\alpha_{out}$, mean calculated heat flux $E$ (in the data acquisition period), calculated heat flux variation $\delta E$ (in the same period), heat flux variation ratio $\delta E/E$, cooling rate $B_{out}$, pulse-related temperature increase $\Delta T_{out}$, thermograph interpolation root mean square residual $R_{out}$, effective signal-to-noise ratio $\Delta T_{out}/R_{out}$.

used [7]. For example, in the present experiment, by modeling the radiative heat transfer with effective surface heat transfer coefficients [7], and by using the above mentioned estimates of the sample's thermophysical properties, this Biot number results always smaller than $2\cdot10^{-3}$. From the lumped capacitance model, it can be obtained:

$$E \approx -\frac{C\cdot\dot{T}}{2\cdot S} \tag{16}$$

and, by a further time derivative,

$$\dot{E} \approx -\frac{C\cdot\ddot{T}}{2\cdot S} \tag{17}$$

where $C$ is the sample's heat capacity and the heat flux from the sample's side surface is neglected. Therefore, if the sample temperature $T$ is observed during the whole cooling process and if (excluding the isolated pulse effects) $\dot{T}$ is always negative and $\ddot{T}$ is always positive, as it usually happens in radiative cooling processes (and actually happened in the reported experiment), it can be concluded that the emissive power $E$ is always positive and its time derivative $\dot{E}$ is always negative.

Moreover, as noted above, the surface heat flux (i.e., the emissive power) can be described as:

$$E = \varepsilon\cdot\sigma\cdot\left(T^4 - T_f^4\right) \tag{18}$$

By recalling that $\dot{E}$ is negative, by differentiating Eq. (18), and because the temperature rate $\dot{T}_f$ of the furnace components in view of the sample is obviously negative, it results that:

$$\begin{aligned}|\dot{E}| &= -\dot{E} = -4\cdot\varepsilon\cdot\sigma\cdot T^3\cdot\dot{T} + 4\cdot\varepsilon\cdot\sigma\cdot T_f^3\cdot\dot{T}_f \\ &< -4\cdot\varepsilon\cdot\sigma\cdot T^3\cdot\dot{T}\end{aligned} \tag{19}$$

and finally, by recalling that $E$ is positive and by combining Eqs. (16) and (19), it results:

$$\begin{aligned}\left|\frac{\delta E}{E}\right| \approx \left|\frac{\dot{E}\cdot\delta t}{E}\right| &= \frac{|\dot{E}|}{|E|}\cdot\delta t < \frac{(-4\cdot\varepsilon\cdot\sigma\cdot T^3\cdot\dot{T})}{(-C\cdot\dot{T}/(2\cdot S))}\cdot\delta t \\ &= \frac{8\cdot\varepsilon\cdot\sigma\cdot S\cdot T^3\cdot\delta t}{C} \equiv D\end{aligned} \tag{20}$$

Therefore, the smaller is the parameter $D$ defined in Eq. (20), the more precise is the adopted analytical model, at least as it regards the constant surface heat flux hypothesis.

Finally, by substituting the $\varepsilon/C$ ratio, as defined in Eq. (14), into Eq. (20), it results:

$$\left|\frac{\delta E}{E}\right| < D = \frac{8\cdot\Delta T\cdot\sigma\cdot S\cdot T^3\cdot\delta t}{Q_i} \tag{21}$$

Therefore, the $D$ parameter can be calculated for each non-standard flash measurement performed during the sample's cooling, by using the average measurement temperature $\overline{\overline{T}}$ (as $T$), the employed laser pulse energy $Q_i$, the calculated $\Delta T$ value, and a relevant duration $\delta t$.

Physically, $D$ depends mainly upon the sample's temperature and is a dimensionless measure of how much the emissive power $E$ would change in time if the sample would be cooling by irradiation at the specified temperature, versus a zero absolute temperature ambient (this latter specification is the physical correspondent of the approximation in Eq. (19)). $D$ does not actually depend upon if and how a flash measurement is performed, because the $\Delta T/Q_i$ ratio is introduced in Eq. (21) only as a mean to measure the $\varepsilon/C$ ratio, which is a sample's own constant. For these reasons, $D$ cannot be employed to estimate $|\delta E/E|$ in the case of standard measurement. Values of $D$ obtained at most investigated temperatures during the cooling stage (Table 2) are lower than 2.5% at the maximum temperature, and steeply decrease while the temperature is decreased. In these calculations, the duration of the data acquisition (2.5 s) was chosen as $\delta t$. Notwithstanding the rough approximations employed, these values (Table 2) are of the same order of mag-

nitude of the above-mentioned $|\delta E/E|$ values obtained from the numerical simulation during the cooling stage (Table 3).

Moreover, for a chosen material and temperature, and by introducing the material's density $\rho$ and specific heat capacity $c_p$, Eq. (20) can be restated as follows:

$$D = \frac{8 \cdot \varepsilon \cdot \sigma \cdot S \cdot T^3 \cdot \delta t}{\rho \cdot c_p \cdot S \cdot L} \propto \frac{\delta t}{L} \tag{22}$$

Because the relevant duration $\delta t$ of an experiment should be proportionate to the specimen's characteristic time $t_c$, and by using the definition $t_c = L^2/(\pi^2 \cdot \alpha)$, from Eq. (22) it follows that:

$$D \propto \frac{\delta t}{L} \propto \frac{t_c}{L} \propto L \tag{23}$$

from which it is apparent that, for a given material and temperature, $D$ scales with the sample's thickness. Therefore the same model may not be acceptable for samples much thicker than those employed in this work.

The variation of the sample thickness $L$, due to the sample's thermal expansion and volumic contraction in respect to its initial (measured) condition, was neglected in the reported calculations. The thermal diffusivity $\alpha$ is proportional to $L^2$ and the maximum total linear variation $\varepsilon_t$ is lower than 0.01 [16], thus the relative error due to the thickness variation is lower than 2%:

$$\frac{\partial \alpha}{\alpha} = 2\frac{\partial L}{L} = 2 \cdot \varepsilon_t < 0.02 \tag{24}$$

Although the calculated thermal diffusivity could be easily corrected for the thickness variation, the reported (uncorrected) values are more consistent with most finite element thermometallurgical models, because these models usually neglect volume variations.

The root mean square residual $R$ of the interpolation theoretically depends upon both the model's likelihood and the noise of the acquired signal. In the present set of experimental measurements, $R$ apparently depends upon the temperature and is insensitive to whether a measurement was performed during a holding or cooling stage (Table 2 and Fig. 5).

The overall likelihood of the proposed analytical model, and particularly the acceptability of the main approximations included in this model (constant thermophysical properties, constant-heat-flux boundary condition, ideal pulse), can also be evaluated by applying the above described data reduction method to the result of the numerical simulations, that were performed without using such approximations (Table 3 and Fig. 6). The root mean square residual $R_{\text{out}}$ obtained by fitting the simulated thermographs (of both standard and non-standard measurements) with the proposed analytical model is lower than $10^{-3}$ K, slightly increasing with the temperature. Moreover, the difference between the diffusivity values obtained from the simulated thermographs and the corresponding input values (values of the diffusivity-vs.-temperature curve employed in the simulation, at the same temperatures) is less than 0.01 $\text{mm}^2\,\text{s}^{-1}$ or 0.2%, (slightly increasing with the temperature in the non-standard cases). Thus, the adopted analytical model is overall satisfying. Nevertheless, the first simulated measurement

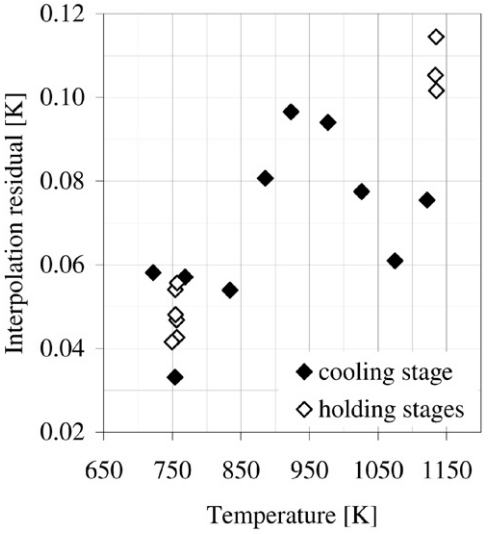


Fig. 5. Mean square residual of the numerical interpolation of the experimental laser flash thermographs, as a function of the temperature. Measurements performed during the cooling or holding stages.

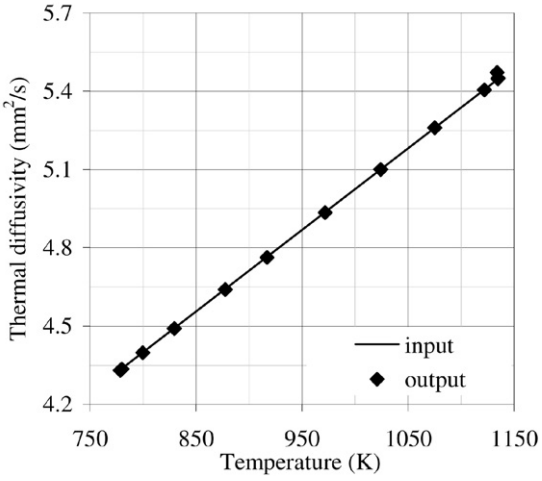


Fig. 6. Thermal diffusivity as a function of the temperature. Input curve employed in the numerical simulation, and output values obtained by interpolating the simulated thermographs with the proposed analytical model.

showed a slightly larger error ($R = 1.9 \cdot 10^{-3}$ K, thermal diffusivity difference 0.035 $\text{mm}^2\,\text{s}^{-1}$ or 0.65%), and the error was always larger in the standard simulated measurement than in those performed during the cooling process. These latter facts can be correlated to the above-mentioned large $\delta E/E$ ratios that occur in the standard measurements (and particularly in the first one), and to the fact that, in the standard measurements, a slow temperature decrease occurs after the pulse instant, but not before. For these reasons, in the standard measurement cases the present model may be slightly inferior in likelihood in respect of, for example, the Cape and Lehman model [28], but still substantially equivalent to the Parker et al. one [22].

By summarizing and comparing the results of the actual and simulated measurements, it can be stated that the adopted analytical model is coherent with both the standard and the non-standard flash measurements, at least in respect to the precision

of the employed measurement apparatus, and that in the experimental cases the residual $R$ is essentially determined by the instrumental noise, rather than by the model's likelihood, because it is always two orders of magnitude larger than the values obtained in the simulated experiments (that depend on the model's likelihood only). Therefore, a more refined model (e.g. a finite elements one) would not yield a significant advantage in the interpolation of thermographs obtained with the present apparatus.

Moreover, because the temperature increase $\Delta T$ is the relevant temperature signal, in the experimental measurements the $\Delta T/R$ ratio can be regarded as a signal-to-noise ratio (this ratio is higher than $10^3$ in the simulated measurements, Table 3).

## Experimental results

During the austenitizing and cooling stages, the measurements performed at the higher temperatures generally showed a larger dispersion (Fig. 7), probably because they presented a worse $\Delta T/R$ signal-to-noise ratio (Table 2) due to an higher noise ($R$ increased approximately from 0.05 to 0.1 K while increasing the temperature from 755 to 1133 K). The measurements performed during the 755 K holding stage showed a much smaller dispersion, because $\Delta T/R$ ratios of the order of 60 were obtained by using higher absorbed pulse energies and thus higher $\Delta T$ temperature increases.

During the 1133 K holding stage, the measurements performed by keeping the heating system working showed negligible cooling rates $B$, thus can be regarded as standard measurements, whereas those performed by switching off the same system just before the measurement showed significant cooling rates, thus should be regarded as non-standard measurements. Nevertheless, the difference between the mean thermal diffusivity values obtained in these two groups of measurements was comparable to the standard deviation observed inside each group. During the 755 K holding stage the differences between the measurements performed with or without the heating system were less evident (Table 2).

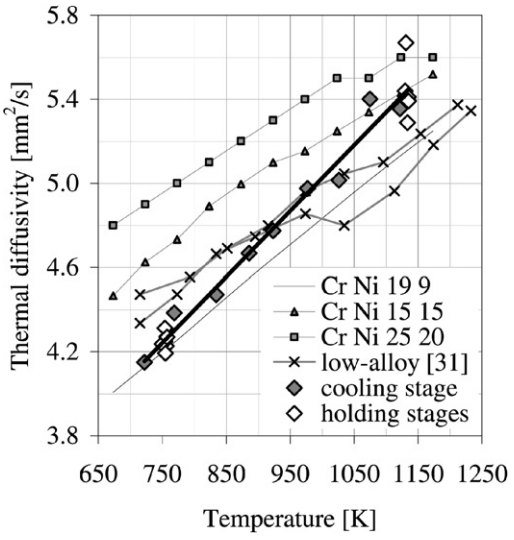


Fig. 7. Thermal diffusivity as a function of the temperature. Measurements performed during the cooling or holding stages and linear interpolation. Previous measurements on a low-alloy austenite [31]. Thermal diffusivity of three austenitic stainless steels with different alloy content.

The thermal diffusivity of the austenite monotonically decreases from about $5.4 \cdot 10^{-6}$ m$^2$ s$^{-1}$ at 1133 K to about $4.3 \cdot 10^{-6}$ m$^2$ s$^{-1}$ at 755 K (Fig. 7). The overall trend of the austenite thermal diffusivity in the investigated temperature range (722 to 1135 K) can be described by the following linear interpolating formula:

$$\alpha = 1.896 + 3.129 \times 10^{-3} T \tag{25}$$

where $\alpha$ and $T$ are expressed in mm$^2$ s$^{-1}$ and K, respectively. This formula (that presents an overall root mean square residual in respect to the measured points equal to about 0.2 mm$^2$ s$^{-1}$) is more precise at the lower end of the investigated temperature range, because both the uncertainty associated with each single measurement and the dispersion of the measured points around the interpolating line increase with the temperature, and because the tests performed on the Armco iron have shown that the instrumental apparatus is less precise at the higher investigated temperatures.

## Discussion and conclusions

The proposed data-reduction method was used to calculate the thermal diffusivity from the thermographs of flash experiments performed upon undercooled austenite samples without prior thermal equilibrium. The results are in reasonable agreement with the standard measurements (at the temperatures at which the latter could be performed) and the same calculations, as well as the results of the numerical simulations, prove that the assumptions used to formulate the underlying analytical model are acceptable in the examined cases.

The thermal diffusivity of the undercooled austenite, as obtained in carbon or low-alloy steels, was previously measured by Solter [31] in the 32NiCrMoV12-3 low-alloy grade.[11] These measurements were performed by using the laser flash method while cooling the specimen from 1273 K to room temperature, whereas the phase transformation was detected only below 715 K, but the employed experimental and data reduction procedures were not reported, and, therefore, it is unclear how the prior thermal equilibrium condition (required by the standard method) was dealt with. Furthermore, in the examined temperature range, some stainless steels present a stable austenitic phase, due to their high alloy (and particularly Nickel) content, and their thermal diffusivity have been extensively studied by standard methods. In Fig. 7 the present results are compared with those reported by Solter and with the previously reported thermal diffusivity of three austenitic stainless steels with different chromium and nickel content: ISO 1.4970 (or X10NiCrMoTiB15-15), containing 15 wt% Cr and 15 wt% Ni [32], AISI 310, containing 25 wt% Cr and 20 wt% Ni [33], and AISI 304, nominally containing 19 wt% Cr and 9 wt% Ni [34].

[11] With the following composition (weigth %): C 0.32, Si 0.14, Mn 0.61, Cr 0.93, Mo 0.46, Ni 2.5.

The present results are overall consistent with those reported by Solter. Moreover, the trend of the thermal diffusivity in respect to the temperature is substantially similar in the low-alloy undercooled austenite and in the three above-mentioned austenitic stainless steels, and the thermal diffusivity values of the low-alloy undercooled austenite are close to those of the less alloyed austenitic stainless steels.

Particularly at the lower investigated temperatures, the thermal diffusivity of the examined undercooled austenite is significantly lower than that of the ferritic constituents (i.e. pearlite, bainite, or martensite) of the same steel [16] and of similar medium-carbon steels [26,31] at the same temperatures. Therefore, a model of a steel's thermal diffusivity, to be employed in a steel quench simulation, should consider the phase dependence of this property.

**Acknowledgements**

Italian Ministry for Education, University and Research, for financial support by research grant PRIN 2003091205. L. Vitrano, H.C.M. Stampi S.p.A., for steel procurement. O. Spilotro, for experimental work performed during his undergraduate thesis.

## Appendix A. Analytical solution of Eq. (3)

The analytical solution of Eq. (3) is described hereafter.

The solution for $t > 0$ can be obtained by using the Laplace transform method [6,23], whereas the solution for $t \leqslant 0$ is obviously zero. By applying the unilateral Laplace transform ($\mathcal{L}_u$) in respect to the variable $t$, the given equations become:

$$\begin{pmatrix} \dot{T}_{\mathrm{III}} = \alpha \cdot T''_{\mathrm{III}}, & x \in [0, L] \\ -k \cdot T'_{\mathrm{III}} = q \cdot \delta(t), & x = 0 \\ -k \cdot T'_{\mathrm{III}} = 0, & x = L \\ T_{\mathrm{III}} = 0, & t = 0 \end{pmatrix} \xrightarrow{\mathcal{L}_u} \begin{pmatrix} s \cdot \theta = \alpha \cdot \theta'', & x \in [0, L] \\ -k \cdot \theta'' = q, & x = 0 \\ -k \cdot \theta'' = 0, & x = L \end{pmatrix} \tag{26}$$

where $s$ is the complex Laplace variable and $\theta(s, x)$ is the Laplace transform of $T_{\mathrm{III}}(t, x)$.

The solution of Eq. (26) in the Laplace domain is:

$$\theta(s, x) = \frac{q}{k \cdot \sqrt{s/\alpha}} \cdot \left[\exp\left(-(2 \cdot L - x) \cdot \sqrt{s/\alpha}\right) + \exp\left(-x \cdot \sqrt{s/\alpha}\right)\right] \cdot \frac{1}{1 - \exp(-2 \cdot L \cdot \sqrt{s/\alpha})} \tag{27}$$

By using the well-known result:

$$\frac{1}{1-y} = \sum_{n=0}^{\infty} y^n, \quad y \in (0,\ 1) \tag{28}$$

and for suitable $s$ values, Eq. (27) can be restated in the following form:

$$\begin{aligned} \theta(s, x) &= \frac{q}{k \cdot \sqrt{s/\alpha}} \cdot \left[\exp\left(-(2 \cdot L - x) \cdot \sqrt{s/\alpha}\right) + \exp\left(-x \cdot \sqrt{s/\alpha}\right)\right] \cdot \sum_{n=0}^{\infty} \exp\left(-2 \cdot n \cdot L \cdot \sqrt{s/\alpha}\right) \\ &= \frac{q}{k} \cdot \sum_{n=0}^{\infty} \left[\frac{\exp(-(2 \cdot (n+1) \cdot L - x) \cdot \sqrt{s/\alpha})}{\sqrt{s/\alpha}} + \frac{\exp(-(2 \cdot n \cdot L + x) \cdot \sqrt{s/\alpha})}{\sqrt{s/\alpha}}\right] \end{aligned} \tag{29}$$

Being known [23] that:

$$\mathcal{L}_u\left\{\left(\alpha/(\pi \cdot t)\right)^{1/2} \cdot \exp\left(-\beta^2/(4 \cdot \alpha \cdot t)\right)\right\} = \exp\left(-\beta \cdot \sqrt{s/\alpha}\right)\Big/\sqrt{s/\alpha} \tag{30}$$

where $\beta$ is a real positive number, the inverse Laplace transform of Eq. (29) is:

$$T_{\mathrm{III}}(t, x) = \frac{q}{k} \cdot \left(\frac{\alpha}{\pi \cdot t}\right)^{1/2} \cdot \sum_{n=0}^{\infty} \left[\exp\left(-\frac{(2 \cdot (n+1) \cdot L - x)^2}{4 \cdot \alpha \cdot t}\right) + \exp\left(-\frac{(2 \cdot n \cdot L + x)^2}{4 \cdot \alpha \cdot t}\right)\right] \tag{31}$$

Finally, by substituting $t_c = L^2/(\pi^2 \cdot \alpha)$ and reordering, it results:

$$\begin{aligned} T_{\mathrm{III}}(t, x) &= \frac{q \cdot \alpha}{k \cdot L} \cdot f_{\mathrm{III}}\left(\frac{t}{t_c}, \frac{x}{L}\right) \\ f_{\mathrm{III}}(\tau, \chi) &= \sqrt{\frac{\pi}{\tau}} \cdot \sum_{n=0}^{\infty} \left[\exp\left(-\frac{\pi^2}{4 \cdot \tau} \cdot \left(2 \cdot (n+1) - \chi\right)^2\right) + \exp\left(-\frac{\pi^2}{4 \cdot \tau} \cdot (2 \cdot n + \chi)^2\right)\right] \end{aligned} \tag{32}$$

for $t > 0$, from which Eq. (7) can readily be obtained by choosing $x = L$ and extending $f_{\mathrm{III}}$ as zero when $\tau \leqslant 0$.

## Appendix B. Verification of Eq. (11)

The integration of $T(t, x)$, as defined in Eq. (9), in respect to $x$, leads to:

$$\begin{aligned} \overline{T}(t) &= \frac{1}{L} \cdot \int_0^L T(t, x)\, \mathrm{d}x \\ &= T_0 + \frac{1}{L} \cdot \int_0^L z(x)\, \mathrm{d}x - B \cdot t + \Delta T \cdot \int_0^1 f_{\mathrm{III}}(\tilde{\tau}, \chi)\, \mathrm{d}\chi \\ &\quad + B \cdot t_c \cdot \int_0^1 f_{\mathrm{II}}(\tau, \chi)\, \mathrm{d}\chi \end{aligned} \tag{33}$$

where $\tilde{\tau} = (t - t_0)/t_c$ and $\tau = t/t_c$.

The function $z(x)$ is a polynomial and therefore its integral is easily calculated; it is:

$$\frac{1}{L} \cdot \int_0^L z(x)\, \mathrm{d}x = 0 \tag{34}$$

Moreover, as it regards the integral of $f_{II}$, by exchanging the summation and the integral, and calculating the latter, it is obtained:

$$\begin{aligned}
&\int_0^1 f_{II}(\tau,\chi)\,d\chi \\
&\quad= \frac{1}{2}\cdot\sum_{n=1}^{\infty}\frac{(-1)^n}{n^2}\cdot\exp\bigl(-4\cdot\tau\cdot n^2\bigr) \\
&\qquad\cdot\int_0^1 \cos\bigl(n\cdot\pi\cdot(2\cdot\chi-1)\bigr)\,d\chi \\
&\quad= \frac{1}{2}\cdot\sum_{n=1}^{\infty}\frac{(-1)^n}{n^2}\cdot\exp\bigl(-4\cdot\tau\cdot n^2\bigr)\cdot\sin(n\cdot\pi)=0
\end{aligned}\tag{35}$$

by considering that $n$ is an integer and therefore $\sin(n\cdot\pi)$ is always zero.

The function $f_{III}$ was assumed to be zero when $\tilde{\tau}$ is negative or zero, therefore:

$$\int_0^1 f_{III}(\tilde{\tau},\chi)\,d\chi=0\quad\text{if }[\tilde{\tau}\leqslant 0]\tag{36}$$

In the opposite case (positive $\tilde{\tau}$), by exchanging the summation and the integral, calculating the integrals of the two Gaussian curves and simplifying, the following series is obtained:

$$\begin{aligned}
&\int_0^1 f_{III}(\tilde{\tau},\chi)\,d\chi \\
&\quad=\sqrt{\frac{\pi}{\tau}}\cdot\sum_{n=0}^{\infty}\left[\int_0^1\exp\left(-\frac{\pi^2\cdot(2\cdot(n+1)-\chi)^2}{4\cdot\tilde{\tau}}\right)d\chi\right. \\
&\qquad\left.+\int_0^1\exp\left(-\frac{\pi^2\cdot(2\cdot n+\chi)^2}{4\cdot\tilde{\tau}}\right)d\chi\right] \\
&\quad=\sum_{n=0}^{\infty}\bigl[\operatorname{Erf}\bigl((n+1)\cdot\pi/\sqrt{\tilde{\tau}}\bigr)-\operatorname{Erf}\bigl(n\cdot\pi/\sqrt{\tilde{\tau}}\bigr)\bigr]\quad\text{if }[\tilde{\tau}>0]
\end{aligned}\tag{37}$$

Every partial sum $S_N$ of this latter series can be calculated by splitting the summation,[12] renumbering a dummy index and simplifying, i.e.:

$$\begin{aligned}
S_N&=\sum_{n=0}^{N}\bigl[\operatorname{Erf}\bigl((n+1)\cdot\pi/\sqrt{\tilde{\tau}}\bigr)-\operatorname{Erf}\bigl(n\cdot\pi/\sqrt{\tilde{\tau}}\bigr)\bigr] \\
&=\sum_{m=1}^{N+1}\operatorname{Erf}\bigl(m\cdot\pi/\sqrt{\tilde{\tau}}\bigr)-\sum_{n=0}^{N}\operatorname{Erf}\bigl(n\cdot\pi/\sqrt{\tilde{\tau}}\bigr) \\
&=\sum_{m=1}^{N}\operatorname{Erf}\bigl(m\cdot\pi/\sqrt{\tilde{\tau}}\bigr)+\operatorname{Erf}\bigl((N+1)\cdot\pi/\sqrt{\tilde{\tau}}\bigr) \\
&\quad-\operatorname{Erf}\bigl(0\cdot\pi/\sqrt{\tilde{\tau}}\bigr)-\sum_{n=1}^{N}\operatorname{Erf}\bigl(n\cdot\pi/\sqrt{\tilde{\tau}}\bigr) \\
&=\operatorname{Erf}\bigl((N+1)\cdot\pi/\sqrt{\tilde{\tau}}\bigr)
\end{aligned}\tag{38}$$

Therefore, the sum of the series can be readily obtained as the limit of the sequence of its own partial sums, i.e.:

$$\int_0^1 f_{III}(\tilde{\tau},\chi)\,d\chi=\lim_{N\to\infty}S_N=\lim_{N\to\infty}\operatorname{Erf}\bigl((N+1)\cdot\pi/\sqrt{\tilde{\tau}}\bigr)=1\quad\text{if }[\tilde{\tau}>0]\tag{39}$$

By unifying Eqs. (36) and (39), it results that the spatial average of $f_{III}$ is the unitary step function:

$$\int_0^1 f_{III}(\tilde{\tau},\chi)\,d\chi=u(\tilde{\tau})\tag{40}$$

and finally, Eq. (11) is readily obtained by substituting Eq. (34), (35) and (40) into Eq. (33).

The same result (Eq. (11)) can be obtained by integrating Eq. (1) in respect to $x$. Moreover, Eq. (11) is confirmed by physical considerations. The spatial average temperature is directly related to the sample's internal energy (trough the sample's heat capacity) and the latter is the sum of an initial value and of the time integral of the heat fluxes, therefore the linear term in Eq. (11) derives from the time integral of the constant cooling heat flux $E$, whereas the step term derives from the time integral of the energy pulse $q\cdot\delta(t-t_0)$.

[12] The series itself cannot be split because the two resulting series would diverge.

## References


[1] C.E. Bates, G.E. Totten, R.L. Brennan, Quenching of steel, in: J.R. Davis, G.M. Davidson, S.R. Lampman, T.B. Zorc, J.L. Daquila, A.W. Ronke, K.L. Henniger, R.C. Uhl (Eds.), ASM Handbook, vol. 4, Heat Treating, ASM Int., Materials Park, OH, USA, 1991, pp. 67–120.

[2] J.L. Lamont, How to estimate hardening depth in bars, The Iron Age (1943, Oct. 14) 64–70.

[3] M.A. Grossmann, E.C. Bain, Principles of Heat Treatment, fifth ed., ASM, Metals Park, OH, USA, 1964.

[4] M. Gergely, S. Somogyi, T. Reti, T. Konkoly, Computerized properties prediction and technology planning in heat treatment of steels, in: J.R. Davis, G.M. Davidson, S.R. Lampman, T.B. Zorc, J.L. Daquila, A.W. Ronke, K.L. Henniger, R.C. Uhl (Eds.), ASM Handbook, vol. 4, Heat Treating, ASM Int., Materials Park, OH, USA, 1991, pp. 638–656.

[5] C.H. Gur, A.E. Tekkaya, Finite element simulation of quench hardening, Steel Res. 67 (1996) 298–306.

[6] G.E. Myers, Analytical Methods in Conduction Heat Transfer, Genium Publ., New York, 1987.

[7] O. Levenspiel, Engineering Flow and Heat Exchange, Plenum, New York, 1984.

[8] E1461-01, Standard test method for thermal diffusivity of solids by the flash method, ASTM, 2001.

[9] ISO 4957:1999, Tool steels, ISO, 1999.

[10] D. Firrao, P. Matteis, G. Scavino, G. Ubertalli, M.G. Ienco, A. Parodi, M.R. Pinasco, E. Stagno, R. Gerosa, B. Rivolta, G. Silva, A. Ghidini, Heat treatment and failure risk of large automotive plastic molds: a fracture mechanics approach and property assessment, La Metallurgia Italiana 98 (11–12) (2006) 43–51.

[11] D. Firrao, P. Matteis, G. Scavino, G. Ubertalli, M.G. Ienco, M.R. Pinasco, E. Stagno, R. Gerosa, B. Rivolta, A. Silvestri, G. Silva, A. Ghidini, Relationships between tensile and fracture mechanics properties and fatigue properties of large plastic mould steel blocks, Mater. Sci. Eng. A (2007), in press.
[12] Thyroplast 2738, Edelstahal Witten–Krefeld steelwork, steel data sheet, 2001.
[13] Keylos 2738, Lucchini steelwork, steel data sheet, 2001.
[14] Bohler M238—The hardened and tempered plastic mould steel, Bohler steelwork, steel data sheet, 2002.
[15] Plastic Mould Steel 2738, Buderus steelwork, steel data sheet, 2000.
[16] E. Campagnoli, D. Firrao, P. Matteis, G.M.M. Mortarino, M. Pavese, G. Ruscica, R. Gerosa, B. Rivolta, G. Silva, Proprietà termofisiche di un acciaio per stampi per materie plastiche, in funzione della temperatura e delle fasi, in: 31° Conv. Naz. AIM (nov. 22–24, 2006). AIM, Milan, Italy, 2006, pp. 163–164 (abstract) and CD-ROM (paper n. 105).
[17] Y.S. Touloukian, R.W. Powell, C.Y. Ho, M.C. Nicolaou, Thermal diffusivity, in: Y.S. Touloukian, C.Y. Ho (Eds.), Thermophysical Properties of Matter, vol. 10, Plenum, New York, USA, 1973, pp. 81–82.
[18] E407-99, Standard practice for microetching metals and alloys, ASTM, 1999.
[19] S.J. Lawrence, Delineating prior austenite grain boundaries in steels, Microsc. Microanal. 10 (Suppl. 2) (2004) 750–751.
[20] S. Bechet, L. Beaujard, Nouveau réactif pour la mise en évidence micrographique du grain austénitique des aciers trempés ou trempés-revenus, Rev. Metall. 52 (1955) 830–836.
[21] E112-96, Standard test methods for determining average grain size, ASTM, 2004.
[22] W.J. Parker, R.J. Jenkins, C.P. Butler, G.L. Abbott, Thermal diffusivity measurements using the flash technique, J. Appl. Phys. 32 (1961) 1679–1684.
[23] H.S. Carslaw, J.C. Jaeger, Conduction of Heat in Solids, Clarendon Press, Oxford, 1959.
[24] J.C. Lagarias, J.A. Reeds, M.H. Wright, P.E. Wright, Convergence properties of the Nelder–Mead simplex method in low dimensions, SIAM J. Optim. 9 (1998) 112–147.
[25] The MathWorks Inc, Matlab, version 6.5.0, software documentation, 2002.
[26] E.A. Brandes, G.B. Brook (Eds.), Smithells Metals Reference Book, Butterworth–Heinemann, Oxford, 1992.
[27] R.D. Skeel, M. Berzins, A method for the spatial discretization of parabolic equations in one space variable, SIAM J. Sci. Statis. Comput. 11 (1990) 1–32.
[28] J.A. Cape, G.W. Lehman, Temperature and finite pulse-time effects in the flash method for measuring thermal diffusivity, J. Appl. Phys. 34 (1963) 1909–1913.
[29] T. Yamane, S. Katayama, M. Todoki, Experimental investigation of nonuniform heating and heat loss from a specimen for the measurement of thermal diffusivity by the laser pulse heating method, Int. J. Thermophys. 18 (1997) 269–290.
[30] A. Cezairliyan, T. Baba, R. Taylor, A high-temperature laser-pulse thermal diffusivity apparatus, Int. J. Thermophys. 15 (1994) 317–341.
[31] H.J. Solter, Changes in thermal diffusivity of the 32 NiCrMoV 12 3 steel associated with phase transitions, High Temp. High Press. 19 (1987) 455–460.
[32] S. Rudtsch, H.P. Ebert, F. Hemberger, G. Barth, R. Brandt, U. Gross, W. Hohenauer, K. Jaenicke-Roessler, E. Kaschnitz, E. Pfaff, W. Possnecker, G. Pottlacher, M. Rhode, B. Wilthan, Intercomparison of thermophysical property measurements on an austenitic stainless steel, Int. J. Thermophys. 26 (2005) 855–867.
[33] J. Clark, R. Tye, Thermophysical properties reference data for some key engineering alloys, High Temp. High Press. 35/36 (2003/2004) 1–14.
[34] R.H. Bogaard, P.D. Desai, H.H. Li, C.Y. Ho, Thermophysical properties of stainless steels, Thermochim. Acta 218 (1993) 373–393.